A novel strain-based health indicator for the remaining useful life estimation of degrading composite structures

Galanopoulos, Georgios; Eleftheroglou, Nick; Milanoski, Dimitrios; Broer, Agnes; Zarouchas, Dimitrios; Loutas, Theodoros

DOI
10.1016/j.compstruct.2022.116579

Publication date
2023

Document Version
Final published version

Published in
Composite Structures

Citation (APA)
Galanopoulos, G., Eleftheroglou, N., Milanoski, D., Broer, A., Zarouchas, D., & Loutas, T. (2023). A novel strain-based health indicator for the remaining useful life estimation of degrading composite structures. *Composite Structures*, *306*, Article 116579. https://doi.org/10.1016/j.compstruct.2022.116579

Composite Structures 306 (2023) 116579

Contents lists available at ScienceDirect

Composite Structures

journal homepage: www.elsevier.com/locate/compstruct

A novel strain-based health indicator for the remaining useful life estimation of degrading composite structures

Georgios Galanopoulos [a], Nick Eleftheroglou [a,b], Dimitrios Milanoski [a], Agnes Broer [b,c], Dimitrios Zarouchas [b,c], Theodoros Loutas [a,*]

[a] Applied Mechanics Laboratory, Department of Mechanical Engineering and Aeronautics, University of Patras, Rio University Campus, 26504 Rio, Greece
[b] Structural Integrity and Composites Group, Faculty of Aerospace Engineering, Delft University of Technology, Kluyverweg 1, 2629HS Delft, the Netherlands
[c] Center of Excellence in Artificial Intelligence for Structures, Aerospace Engineering Faculty, Delft University of Technology, the Netherlands

ARTICLE INFO

Keywords:
Structural health monitoring
Composite structures
Fiber Bragg grating sensors
Health indicators
Genetic algorithms
Remaining Useful Life prediction

ABSTRACT

We present a generic methodology for developing a Health Indicator out of strain-based Structural Health Monitoring data suitable for implementation in prognostic tasks. For this purpose, an in-house test campaign is launched. Single-stringered composite panels are subjected to compression-compression fatigue with the strains being monitored with Fiber Bragg Grating sensors located along the stringers' feet. Three different fatigue scenarios with increased complexity are investigated i.e. constant amplitude fatigue, variable amplitude fatigue and finally random amplitude (spectrum) fatigue. In this paper, we propose a fusion scheme based on Genetic Algorithms, with the resulted fused Health Indicator achieving high monotonicity and prognosability, both crucial attributes for an enhanced performance of prognostic algorithms. Finally, a popular machine learning algorithm, i.e. Gaussian Process Regression, is employed in order to predict the Remaining Useful Life of the panels in the test set. It is evidenced that the newly proposed fused Health Indicator predicts the Remaining Useful Life far more accurately as several popular performance metrics indicate. The methodology retains a data agnostic character able to be applied in Structural Health Monitoring data from different sensing technologies.

1. Introduction

With composite structures having increased use in the aerospace industry [1], it is important to find effective and efficient ways to monitor their degradation. The main challenge with these materials is their inhomogeneous nature which makes their degradation behavior and failure mechanisms difficult to interpret, understand and model. During their service lifetime these structures are being subjected to a variety of different loading and environmental conditions, as well as unexpected events, such as tool drops or bird strikes, which can significantly reduce their load bearing capability. Barely visible impact damage (BVID) poses a grave risk for these structures, since such impacts usually remain undetected during routine inspections, whilst having a significant effect on the integrity of the structure. Hence, advanced monitoring technologies need to be implemented to monitor their degradation behavior.

Structural Health Monitoring (SHM) technologies have recently captured the interest of many researchers for allowing real time monitoring of entire structures or localized areas [2,3], in order to detect, locate and quantify the degradation of the structure [4,5,6]. The ultimate level of SHM is the prediction of the Remaining Useful Life (RUL) a topic rather still in its infancy. The utilization of SHM data for prognostics is considered one of the most demanding tasks to achieve [7,8]. Of central importance is RUL which is at the epicenter of every prognostic task [9]. RUL prognosis is often associated with diagnostics and accurate predictions are affected by the knowledge of the degradation state, as measured from the SHM systems [10].

Over the years, several prognostic methodologies for RUL estimation have been presented which can be roughly classified into two major categories [11,12]. First, there are model-based prognostics, where a mathematical model describing the physics of the part or structure is required which is used to predict the degradation up to a certain point, i.e. the End-of-Life threshold. Secondly, there are data-driven prognostic methodologies that rely on statistical models or Machine Learning (ML) algorithms and are dependent on the existence of historical run-to-failure data. A common data-driven prognostic framework consists of

* Corresponding author at: Applied Mechanics Laboratory, Department of Mechanical Engineering and Aeronautics, University of Patras, Rio University Campus, 26504 Rio, Greece.
E-mail address: thloutas@upatras.gr (T. Loutas).

https://doi.org/10.1016/j.compstruct.2022.116579
Received 22 June 2022; Received in revised form 4 November 2022; Accepted 6 December 2022
Available online 10 December 2022

four steps: 1. Data acquisition, 2. Health indicator construction, 3. Modeling the degradation process, and finally 4. RUL estimation [12]. The SHM measurements obtained during service are used to feed the ML algorithms or statistical models which have been trained on historical data, to provide estimations of the RUL. A number of model-based studies for RUL estimation using stiffness and energy-based models have been proposed [13–17], however data-driven methods are more suitable for complex composite structures, since model-based methods rely on several assumptions to efficiently model a composite material's degradation and their implementation is impossible in most real life applications [18]. Stochastic processes such as Markov models and non-linear regression algorithms are common data-driven algorithms that usually are employed for prognostics in composites. For instance, Eleftheroglou et al. [8] proposed a nonhomogeneous hidden semi Markov model (NHHSMM) for RUL estimation of open-hole composite coupons subjected to constant amplitude tension–tension fatigue. Acoustic emission (AE) data were used to train the NHHSMM for RUL prognosis of the coupons. The damage states of the model were estimated via a cross-validation and maximum likelihood estimation scheme. The RUL was predicted with great accuracy demonstrating the potential of the framework for integration in different SHM datasets. In [19] a fusion of AE and DIC strain data was proposed to improve the prognostic capabilities of the NHHSMM. It was observed that even though the fused data had a more monotonic behavior, it did not always provide more accurate RUL estimations. Cristiani et al. [3] used strain sensors, specifically FBGs, to monitor delamination growth of double cantilever beam specimens during fatigue. A Particle Filter algorithm is used to estimate the degradation state and delamination extent and ultimately estimate the RUL. Liu et al. [20] also utilized AE data as well as data from lamb waves to predict RUL in composite beams. A Gaussian process model was trained using a normalized damage index to perform non-linear regression for RUL prediction. Comparing the two RUL estimations, the AE-based estimations displayed slightly better estimation results. The same group [21] displayed the prognostic capabilities of a Gaussian process for nonlinear regression on the estimation of the RUL of composite coupons subjected to uniaxial and biaxial constant amplitude fatigue. Real-time sensor data from strain gauges were collected and used to predict the RUL of the composites.

Health indicators (HIs) are damage-sensitive features extracted from raw SHM data. They are a crucial element of data-driven structural diagnostics and prognostics. The quality of the HIs affects substantially the performance and accuracy of prognostic algorithms [22]. There are three main qualities that a candidate HI for prognostic purposes must possess, i.e. monotonicity, prognosability and trendability [23,24], which are closely linked with the accuracy of the predictions. In literature, HIs are classified into two categories [25,26] i.e. HIs which are a result of simple calculations between physical measurements like strain or temperature, namely physical HIs (pHIs), and HIs which are extracted via complex data manipulation and usually lack direct physical meaning, namely virtual HIs (vHIs). Exemplary, signal Root Mean Square (RMS) [27,28] has been used as a pHI in bearings' RUL prediction. On composite materials and structures, pHIs have been developed out of strain data extracted from both finite element models (FEM) as well as experimental data in [29,30]. The HIs were able to capture disbond growth in stiffened panels during quasi-static loadings. VHIs are developed to obtain desirable properties for their monitoring applications. Principal Component Analysis (PCA) has been used as a methodology to create vHIs. Loukopoulos et al. [31] and Loutas et al. [22] used PCA, more specifically Q index and T^2, as HIs to monitor the degradation of reciprocating compressors. Multiple ML models were then used to predict the RUL of the compressors using these two HIs. Shahid et al. [32] proposed a HI based on a dimensionality reduction technique and then utilized a radial basis function to normalize the HI to [0,1]. The HI's performance was demonstrated on data from aircraft engines. Galanopoulos et al. [33] proposed both pHIs and vHIs from strain and acoustic emission data recorded during compression fatigue of single stiffened composite panels. The HIs displayed highly monotonic behaviors with the evolution of damage, though the prognosability was rather low. Yang et al. [34], proposed a mapping of the health status to a linear HI using Neural Networks (NN) for the prediction of RUL in electrical motors. Dynamic smoothing was applied to the HI to improve the monotonicity, consistency and gradualness. Though the RUL prediction results were good, the assumption of linear degradation oversimplifies the problem and cannot capture the stochasticity that usually presents in more complex applications. To address this shortcoming, Song et al. [35] proposed a kernel-based data fusion model, which relaxes the linear assumption, i.e. the raw data are mapped to the feature space using a non-linear kernel function, and this can better model the intricate relationships between the sensor data and the degradation process. In [36], a HI is proposed to indicate the health state of batteries. To enhance the HI, a Box-Cox transformation is applied to improve the correlation to the actual health state. In [37] a composite HI is proposed based on feature level fusion using an optimization scheme that aims to maximize three attributes, i.e. monotonicity, trendability and robustness. A linear combination of these three features is proposed as the fitness function of a Self-Adaptive Differential Evolution algorithm which is used to calculate the weights of each feature during the fusion process. The effectiveness of this HI is demonstrated in two different datasets i.e., bearings and batteries datasets. A different approach for HI construction was followed in [38]. The HI formulation, expressed in flight hours, is based on the effect (either positive or negative) of the chosen degradation features on the health state of the system. The effect is determined based on irregularities found in the sensor data, when compared to the reference measurements. Nguyen and Medjaher [39], proposed a HI based on a two-stage Genetic Programming methodology. In the first stage, automated feature extraction is performed based on multiple evaluation criteria, such as monotonicity and trendability. In the second stage, the extracted features in stage one are fused together to create an enhanced HI. The applicability of the methodology is presented in two distinct datasets, bearing signals and aircraft engine signals.

While there have been several methodologies proposing prognostic HIs from condition monitoring of machinery or systems, few works have focused on SHM data from composite material or structural components towards the development of useful prognostic HIs out of them. Even fewer have worked with geometries beyond simple rectangular coupons. In this paper, we attempt to fill this gap and valorize complex SHM data from fatigue tests in generic structural elements i.e. single-stringered panels towards creating HIs suitable for prognostics. More specifically, we propose a feature-level fusion of physical and virtual strain-based HIs using Genetic Algorithms to create a new HI for RUL prediction of composite panels. The goal of the fusion is to develop a HI with high monotonicity and prognosability, since these two metrics are considered important for accurate RUL estimations. SHM data acquired after three different experimental campaigns are utilized to this direction. The training process of the Genetic Algorithm and the prognostic model is implemented using a subset of the tested panels, while the remaining panels are used to validate the methodologies and demonstrate the capabilities of the proposed methodology. Our expectation that such a HI would be able to provide more accurate prognostics is evidenced and discussed. The concept of the present paper is schematically depicted in Fig. 1.

The remainder of the paper is organized as follows. Section 2 provides insights into the experimental campaigns and the test specimens, Section 3 discusses the methodologies for the HI fusion and prognostic algorithm, while Section 4 displays the fused Health Indicator and the RUL predictions. Finally, the paper is concluded in Section 5.

2. Experimental campaign

CFRP panels were manufactured out of IM7/8552 unidirectional prepreg material. A single *T*-shaped stiffener was used to reinforce the

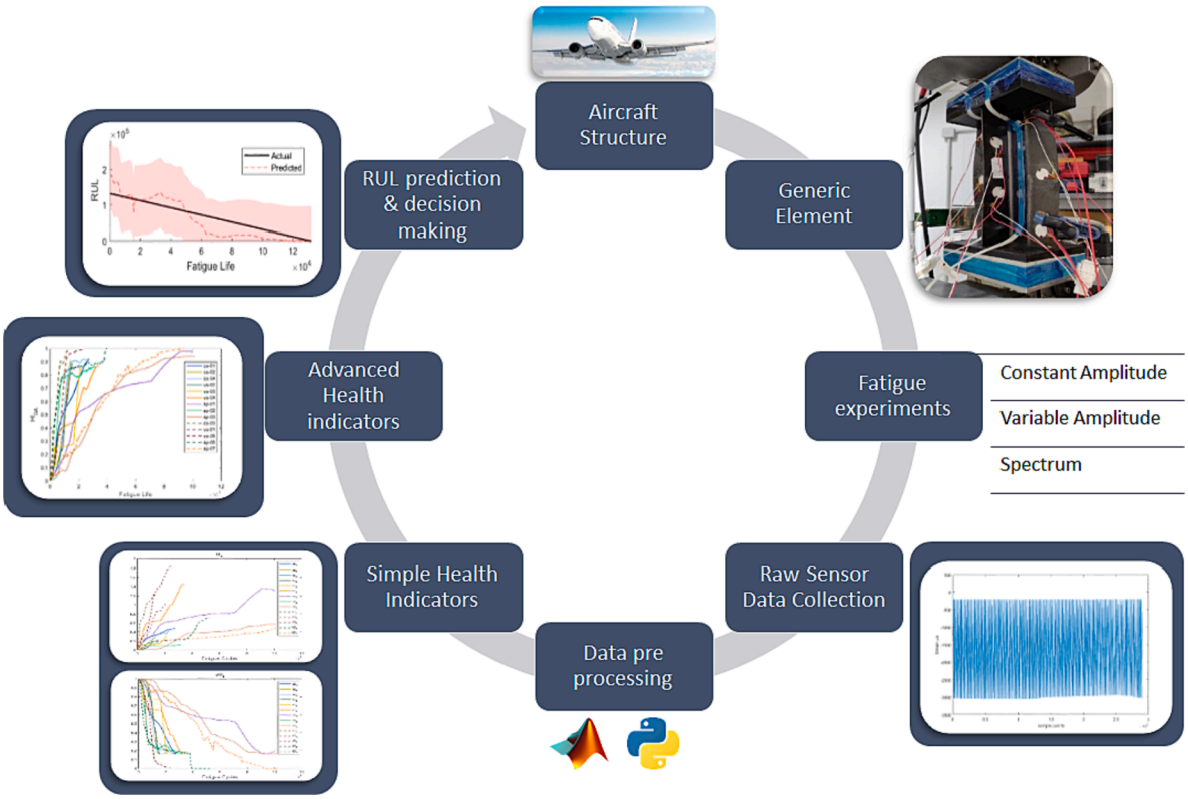

Fig. 1. Schematic representation of the proposed framework.

panel. Skin and stringer are co-cured. The respected layups for the skin and stiffener are $[45/-45/0/45/90/-45/0]_S$ and $[45/-45/0/45/-45]_S$. After the manufacturing, resin cast tabs are added to the free edges of the panels to ensure a proper and uniform compressive load introduction.

First, static tests were conducted on pristine panels to evaluate the ultimate compressive strength and guide our decision towards selecting the fatigue loads. The average compressive strength was calculated at around 100 kN [40]. Before being subjected to fatigue, an initial damage was introduced to the panels at various locations along the stiffeners' feet; either via a manufacturing defect in the form of an artificial disbond using a Teflon insert or as low-velocity impact damage. More information regarding the damage sizes as well as the panels' ultimate fatigue life until collapse is presented in detail in Tables 1-4.

Several sensors were mounted on the panels to monitor their fatigue behavior, e.g. lamb wave PZTs, AE sensors, and FBG strain sensors. The panels' dimensions and sensor locations can be seen in Fig. 2. In the present work, we only focus on strain data collected from the FBGs. The FBG sensors are enclosed in a SMARTape™ [41] that eases handling, a courtesy of Smartec S.A. (Switzerland). Two SMARTapes, one at each stiffener foot, are bonded in each panel using a copolyamide-based adhesive. Each SMARTape contains 5 FBG sensors with a sensor spacing of 20 mm. The measurement area was focused on the middle section of the panels for a length of approximately 140 mm since the damage scenarios concern this area.

Strain measurements are an efficient way of monitoring degradation

Table 1
Constant amplitude test campaign specimen information.

Specimen #	Impact Energy/Disbond Size	Load (kN)		# of Cycles to failure
		Min.	Max.	
CA-1	10 J	−6.5	−65	280,098
CA-2	10 J	−6.5	−65	144,969
CA-3	10 J	−6.5	−65	133,281
CA-4	30x20 mm^2	−5.0	−50	438,000
		−6.0	−60*	

*load increased after 100 k cycles.

Table 2
Variable amplitude test campaign specimen information.

Specimen #	Impact energy/ disbond size	Load (kN)		# of cycles to failure
		Min.	Max.	
VA-1	7.4 J	−4.0	−40	10,000
		−4.5	−45	80,000
		−5.0	−50	30,000
		−5.5	−55	70,000
		−6.0	−60	12,300
				202,300
VA-2	10 J	−4.0	−40	10,000
		−4.5	−45	80,000
		−5.0	−50	90,000
		−5.5	−55	63,000
				243,000
VA-3	10 J	−4.0	−40	10,000
		−4.5	−45	177,000
		−5.0	−50	30,000
				217,000
VA-4	25x20 mm^2	−3.5	−35	10,000
		−3.9	−39	10,000
		−4.5	−45	10,000
		−5.0	−50	170,000
		−5.5	−55	85,000
		−6.0	−60	60,000
				345,000
VA-5	7.37 J	−4.0	−40	20,000
		−4.5	−45	75,000
		−5.0	−50	25,000
		−5.5	−55	62,000
		−6.0	−60	60,000
				242,000

Table 3
Spectrum fatigue load and cycles (modified TWIST algorithm).

Cycles	Min load (kN)	Max load (kN)	Ratio
1	−8.0	−78.0	9.75
2	−5.0	−75.0	15.00
5	−9.0	−69.0	7.67
18	−4.5	−64.5	14.33
52	−4.7	−59.7	12.70
152	−4.8	−55.2	11.50
800	−9.6	−50.4	5.25
4170	−14.1	−45.9	3.25

for two reasons. First, strain is affected by a global stiffness reduction which can provide an indication of degradation over time, and secondly, strain is sensitive to damage, and especially in the vicinity of the damaged area, the strain field is significantly affected [42,43,44,45]. Since FBGs are an optical sensing methodology, the conversion from wavelength to strain is made using eq. (1), where $\Delta\lambda$ is the change from the central wavelength and $f_g = 1.2$ is the gauge factor.

$$\varepsilon = \frac{\Delta\lambda}{\lambda_o} f_g \tag{1}$$

2.1. Fatigue experiments

Three different experimental campaigns in fatigue were conducted [46]. The panels were subjected to constant, variable and finally random amplitude (spectrum) fatigue; a more realistic loading scenario. The fatigue loads ranged from 45 % to 85 % of the ultimate compression strength. The frequency of the loading was 2 Hz and the load ratio, for the constant and variable amplitude fatigue, was kept to 10.

2.1.1. Constant amplitude fatigue

The constant amplitude fatigue test campaign was performed in the Aerospace Structures and Materials Laboratory of Delft University of Technology, on an MTS hydraulic machine with a load capacity of 500 kN. Every 500 cycles, the fatigue test was interrupted and quasi-static loadings were conducted from the minimum to the maximum load, during which the FBG strains were measured. The FBG sensors recorded the entire quasi-static using a Micron Optics sm130 2-channel dynamic interrogator with an acquisition rate of 5 Hz. Table 1 summarizes the tests performed and the cycles to failure.

2.1.2. Variable amplitude fatigue

The second test campaign was conducted in the Applied Mechanics Laboratory of the University of Patras, on an Instron 8802 hydraulic machine with a load capacity of 250 kN. The load was increased after applying blocks of constant loading and observing the damage evolution using the C-scan images from a phased array camera approximately every 10 k cycles. Every 500 cycles quasi-static loadings were conducted from the minimum to maximum fatigue load, when FBG measurements were recorded. The acquisition hardware and sampling rate for strain measurements are the same as in the constant amplitude fatigue campaign. Table 2 summarizes the tests performed and the cycles to failure.

2.1.3. Spectrum fatigue

The final test campaign was also conducted in the Applied Mechanics Laboratory of the University of Patras. A modified version of the TWIST algorithm [47] was used to create the loading sequence. The loads and cycles they were applied for are shown in Table 3. The FBG measurements were recorded at 20-*sec* intervals happening every 7 min, capturing the strains during fatigue, with an acquisition rate of 10 Hz. Phased array C-scan images were also taken approximately every 10 k-20 k cycles to inspect damage evolution, and the load sequence was altered if no damage growth was observed. The sequence was changed by introducing harsher conditions by either adding cycles at higher loads or increasing the amount of cycles the higher loads are applied. Table 4 summarizes the tests performed and the cycles to failure.

3. Methodologies

A variety of different experiments were performed, with different initial damage, different loading sequences and damage accumulation evidence. Hence, a common ground must be established regarding the raw strain data processing to further convert them in a form that better reflects the damage evolution phenomenon of the CFRP panels. For the constant and variable campaigns due to the different loading conditions, the following pre-processing method was implemented which is described in detail in [33] and is briefly mentioned here. From each quasi-static loading, n random strain points were sampled using a uniform distribution and the average of these points was considered as the strain at that time instance. For the spectrum campaign, a total of 30 random strain measurements were selected over the 20 sec measurement window, and their average strain value was used as the strain at that time instance. For the constant and variable amplitude fatigue

Table 4
Spectrum test campaign specimen information.

Coupon	Impact energy/ disbond size	Max load interval (kN)	# of cycles to failure
SP-1	10 J	−50.4 to −75.0	1,000,000
		−50.4 to −78.0	580,000
			1,580,000
SP-2	10 J	−50.4 to −69.0	291,000
		−50.4 to −78.0	238,000
			529,000
SP-3	10 J	−50.4 to −78.0 (pristine)	60,000
		−50.4 to −78.0 (impact)	240,000
		−55.2 to −78.0	300,000
		−55.2 to −82.0	600,000
			1,300,000
SP-5	10 J	−45.9 to −64.5	247,000
		−45.9 to −69.0	92,000
		−45.9 to −75.0	10,000
		−50.5 to −75.0	73,000
		−50.4 to −78.0	30,000
			452,000
SP-7	25x20 mm^2	−55.2 to −78.0	460*
		−45.9 to −59.7	1,160,000
			1,160,460

*disbond doubled in size.

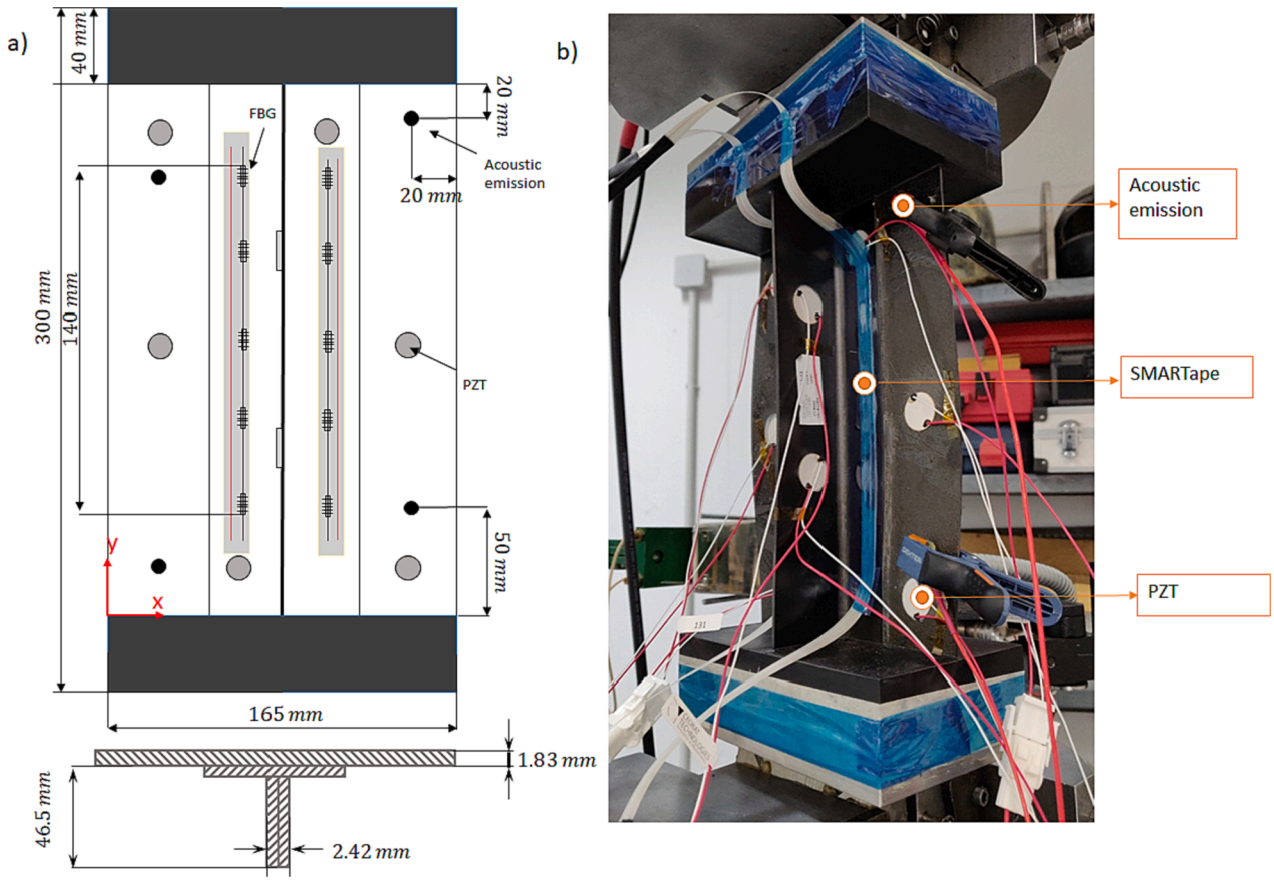

Fig. 2. a) Panel dimensions and sensor locations and b) photo of the panel inside the hydraulic machine.

campaigns, the time instance corresponds to the cycles at the beginning of the quasi-static, while for the random amplitude, the time instance corresponds to the cycle at the beginning of the measurement. After modifying the raw strain data into a common form, advanced processing methodologies are applied to create HIs capable of reflecting the degradation during fatigue.

3.1. Genetic algorithm fusion

In our previous work in [33], some HIs developed out of raw strain data showed potentiality as prognostic features. They are repeated in eq. 2–8 for the sake of completeness. Physical indicators HI_3 and HI_4 are an advancement of HI_1 and HI_2 respectively, where HI_1 measures the strain deviation from the reference state and HI_2 shows the effect of each sensor's measured strain at the mean strain at the sensor's foot. Virtual indicators such as vHI_1, vHI_2 and T^2 do not have an immediate correlation to physical measures, though they have demonstrated good prognostic potential in [31,32].

$$HI_1^i(t) = \frac{\left|\varepsilon_{ref}^i - \varepsilon^i(t)\right|}{\left|\varepsilon_{ref}^i\right|} \tag{2}$$

$$HI_2^i(t) = \frac{\varepsilon^i(t)}{\frac{\sum_1^n \varepsilon^i(t)}{n}} - \frac{\varepsilon^i(t=0)}{\frac{\sum_1^n \varepsilon^i(t=0)}{n}}, t > 0 \tag{3}$$

$$HI_3(t) = \sqrt{\sum \left(M_i HI_1^i(t)\right)^2} \tag{4}$$

$$HI_4(t) = \sqrt{\sum \left(M_i HI_2^i(t)\right)^2} \tag{5}$$

$$\mathrm{vHI}_1(t) = \exp\left(-\frac{(d_L(t) - d_{Lmin})^2}{\sigma_L}\right),$$

Where,

$$\sigma_L = -\frac{(d_{Lmax} - d_{Lmin})^2}{2}\left[\frac{1}{\log 10\varepsilon} + \frac{1}{\log 10(\varepsilon + \delta)}\right] \tag{6}$$

$$vHI_2(t) = \sum_1^N (x_i(t) - x_{r_i}(t))^2 \tag{7}$$

$$T^2(t) = \sum_1^N \frac{\tau_i^2(t)}{\lambda_i} \tag{8}$$

With i = 1,…,N the i^{th} FBG sensor is noted, ε_{ref} is the strain at reference state, $\varepsilon(t)$ is the strain at time t and M_i the monotonicity (see eq. (10)) of each HI curve. d_L, d_{Lmin} and d_{Lmax} are the Euclidean distances of the transformed data from the initial point (at t = 0), while ε and δ are length and scale parameters and are set to 0.1. $x_i(t)$ and $x_{r_i}(t)$ are the original and reconstructed data, extracted from PCA at time *t and* λ_i and τ_i, are the variance and score of the i^{th} principal component. For more information regarding the HIs the interested reader is referred to [31–34].

For an HI to possess prognostic potentiality, three attributes i.e. monotonicity, prognosability, and trendability need to be as high as possible [19,23,24]. Monotonicity results from the fact that the damage is continuously growing and cannot return to a previous damage state, unless a maintenance action is performed, hence the HI should as well constantly increase, or decrease. Trendability, indicates how similar is the underlying trend of a HI for a population of similar structures. Last but not least, prognosability, measures the scatter of the failure values of

the HI for a population of similar structures. In our work we focus mainly on monotonicity and prognosability. Trendability is not considered as important in this work since modern algorithms can adequately model any kind of underlying degradation trends.

For the calculation of the aforementioned attributes, we considered the definitions proposed in [48]. Their values range from [0,1], where 1 indicates the perfect and 0 is the less satisfactory level of a specific attribute.

The average monotonicity for a population of N similar structures is defined as:

$$Monotonicity = \frac{1}{N}\sum_{i=1}^{N} M_i \tag{9}$$

where M_i is the monotonicity of a HI for a single structure, expressed by:

$$M_i = \frac{n_i^+}{n_i - 1} - \frac{n_i^-}{n_i - 1}, i = 1, \cdots, N \tag{10}$$

where n_i^+ and n_i^- the number of positive and negative first derivatives of the HI curve and n_i the total number of observations of this HI. Usually, prognostic features are noisy and proper smoothing is required before calculating the monotonicity, but in our case, there was no such need.

Prognosability, is defined as the standard deviation of the HI failure values of the available lifetimes, divided by the average variation between the values of the HI at the start and end of the lifetime (failure value). To ensure the scale is between [0, 1] the metric is exponentially weighted.

$$Prognosability = \exp\left(-\frac{std\left(HI_{fail}\right)}{mean\left(\left|HI_{start} - HI_{fail}\right|\right)}\right) \tag{11}$$

where HI_{start} and HI_{fail} are the HI values at the beginning and end of the specimens' lifetimes.

Fig. 3 shows the prognosability and average monotonicity of the five HIs of eq. 4–8. We can observe that most HIs possess high monotonicity, however prognosability is rather low. To remedy this shortcoming, we propose an optimization scheme in order to fuse the available HIs into a superior HI_{GA} with maximum monotonicity and prognosability. HI_{GA} will be presented in detail in section 4.1 and is only shown here for comparison purposes.

Genetic algorithms (GAs) were selected over other optimization methods since they have been previously used successfully for prognostics feature extraction in condition monitoring of machinery and systems [48–51]. GAs provide great flexibility in discovering new mathematical equations, can easily account for multiple evaluation criteria and are able to accomplish accurate results without the need for understanding the underlying physics of the structure under investigation [39]. The underlying process is also easily understood providing great oversight of the overall optimization procedure. GPLAB [52] for MATLAB was preferred over other toolboxes due to its capabilities and ease of adding and implementing new functions.

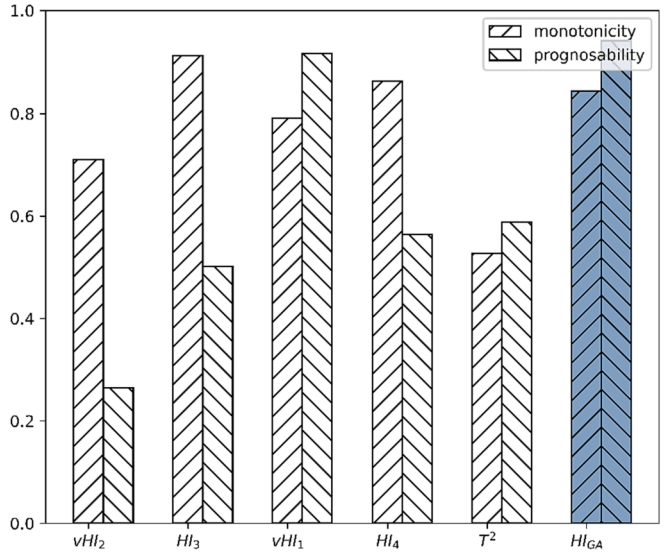

Fig. 3. Monotonicity and Prognosability of existing and proposed HI.

A schematic representation of the fusion process can be seen in Fig. 4. The panels are split into training and testing sets. The training set is used to learn the GA parameters and extract the fusion function. For the training of the GA, three arbitrary panels from each campaign (3xCA, 3xVA and 3xSP) were selected, while the rest were left out for testing. Also, for the case of vHI_1, prior knowledge of minimum and maximum values is required. To this end, vHI_1 for the test set is calculated as follows: first vHI_1 for the training specimens is calculated and the normalization parameters are saved. Then a k-nearest-neighbors scheme is implemented, which is searching for similarities between the initial values of the test panels and the training database. Arbitrarily, the averaged 3-Nearest Neighbors normalization values were used for the calculation of vHI_1 for the test set. Then the GA module is introduced. After initializing the parameters and creating the initial population, the genetic operations are performed to create the subsequent generations. The algorithm finishes when either the max generations are reached, or a perfect fitness result is achieved. Finally, the best output function of the GA is used to create a fused HI.

A variety of different parameter combinations were investigated during the GA fusion process. The three main parameters investigated were sampling, expected, and elitism. Sampling refers to which population of individuals are selected to have children. Expected refers to the expected number of children that each individual creates. Finally, elitism refers to the chances of survival of each individual and children to the next generation. The allowed operations between the inputs are addition, subtraction, multiplication, division, squared power, square root and logarithm. The population of each generation was set to 150 and the maximum generations (iterations) were 300. The population size was chosen with regard to the computational time, while at the same time not compromising possible fusion scenarios, while the iteration limit was chosen based on the convergence of the fitness function (it was observed that when reaching 300 iterations the fitness values had stabilized). The maximum tree depth was limited to 15 so that the obtained functions are not extremely large. The computational time of each run (each parameter combination) is approximately 7 min in MATLAB 2021, running on an Intel quad-core i5-4690k with 16 GB ram. The final selection was mainly guided by the size and the simplicity of the fusion function (number of terms in each operation, total number of terms), since many different fusion schemes managed to provide HIs with high fitness values.

We use the fitness function described in eq. (12) as an objective function to be maximized utilizing the GA optimization technique.

$$Fitness = a^*Monotonicity + b^*Prognosability \tag{12}$$

It was decided to give both properties equal weighting i.e., $a = b = 1$ since both are considered equally important.

3.2. Prognostics – Gaussian process regression

Gaussian processes (GPs) have been widely employed for RUL prognosis of a variety of systems [53–55] and structures [20,21] in a non-linear regression approach. Non-linear regression for RUL estimation has been utilized also in [5] via Bayesian Neural Networks. A GP is a finite collection of random variables indexed by time or space with a joint Gaussian distribution and is a function of $f(x)$ at $x = [x_1, x_2, \ldots, x_n]^T$, where x the collection of random variables. A GP is completely specified [56] by its mean function:

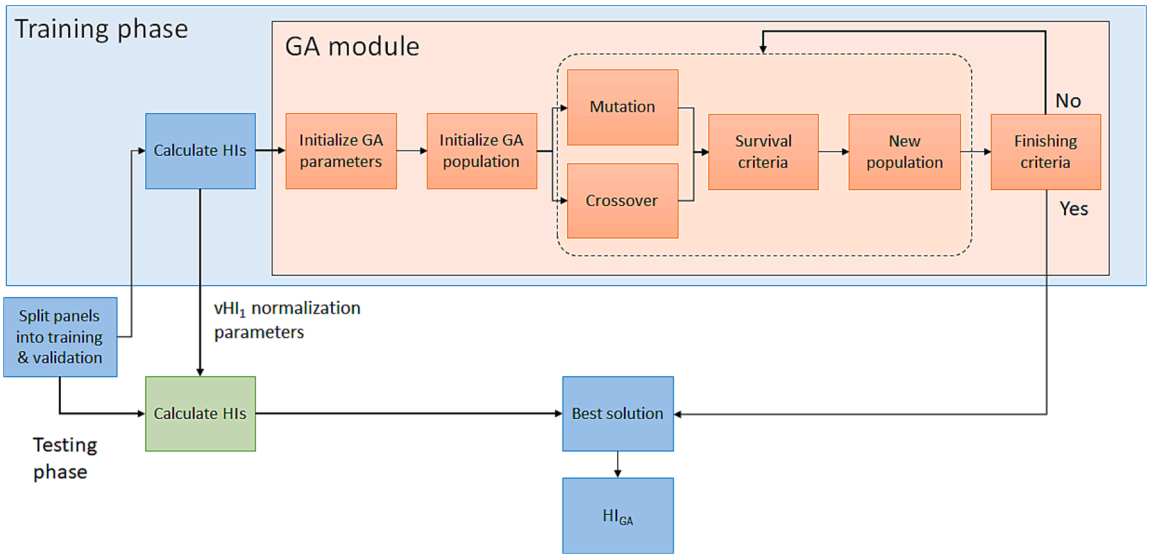

Fig. 4. Flowchart of the proposed fusion methodology.

$$m(x) = E[f(x)] \tag{13}$$

And its covariance function:

$$k(x, x') = E[(f(x) - m(x))(f(x') - m(x'))] \tag{14}$$

Based on the aforementioned equations, i.e. eq.13 and eq.14, the GP can be written as:

$$f(x)\ GP(m(x), k(x, x')) \tag{15}$$

Depending on the data, different covariance functions can be applied in order to best characterize the relationship between x and x'. To investigate the effects of the mean and covariance functions, one of the test panels was used for tuning these two parameters, w.r.t. reducing the error between predicted and actual RUL. Different combinations of mean and covariance functions were tested, and a linear mean function and a Matern 5/2 covariance function were eventually used.

$$m(x) = c_1 x + c_0 \tag{16}$$

$$k(r) = \sigma_f^2 \left(1 + \frac{\sqrt{5}\, r^2}{\sigma_l^2} + \frac{5r^2}{3\sigma_l^2}\right) \exp\left(-\frac{\sqrt{5}\, r}{\sigma_l}\right) \tag{17}$$

where σ_f and σ_l are the standard deviation and scale length respectively, and r is the Euclidean distance between x and x'.

Let us assume a degradation history $H = [x_i, y_i]_{i=1}^N$, where x_i is the input variable and $y_i = f(x_i) + \varepsilon_i$ is the noisy target variable, with ε_i is an independent and identically distributed (*i.i.d*) variable with 0 mean and σ_n^2 ($\varepsilon_i \sim$ *i.i.d* $N(0, \sigma_n^2)$). The joint distribution of the observed target values $y = [y_i]_{i=1}^N$ and unobserved target values f^* at new input locations X^* can be denoted as:

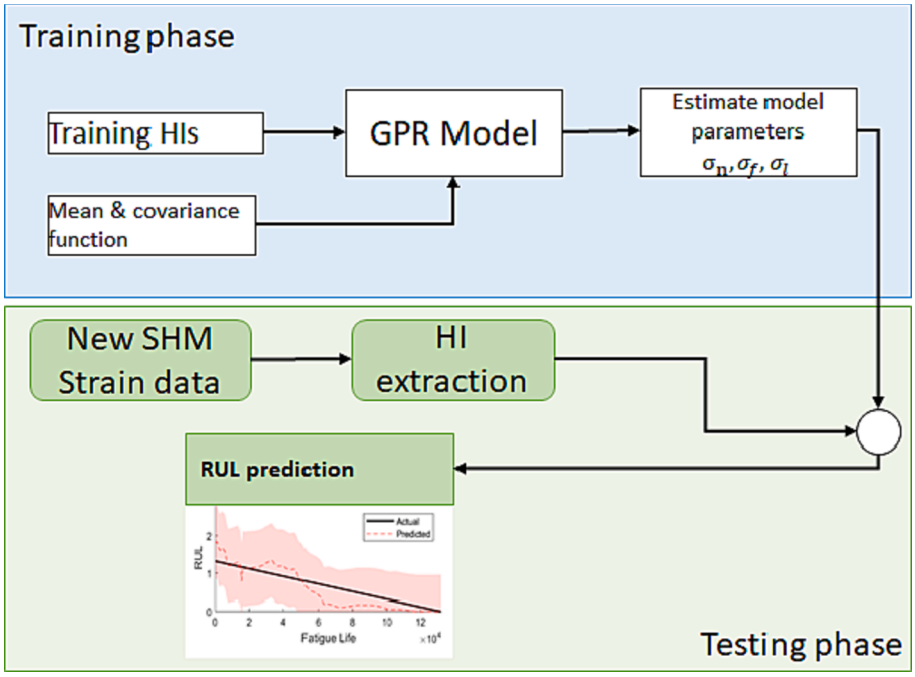

Fig. 5. Schematic representation of the GP training and testing process.

$$\begin{bmatrix} y \\ f^* \end{bmatrix} N \left(0, \begin{bmatrix} K(X,X)+\sigma_n^2 I & K(X,X^*) \\ K(X^*,X) & K(X^*,X^*) \end{bmatrix} \right) \tag{18}$$

where I the identity matrix. The predictive (posterior) distribution for GP regression (GPR), given the new inputs X^* and the historic data X and targets y is defined by:

$$p(f^*|X,y,X^*)\ N(\overline{f^*}, cov(f^*))\ ) \tag{19}$$

$$\overline{f}^* = E[f^*|X,y,X^*] = K(X^*,X)\left[K(X,X)+\sigma_n^2 I\right]^{-1} y \tag{20}$$

$$cov(f^*) = K(X^*,X^*) - K(X^*,X)\left[K(X,X)+\sigma_n^2 I\right]^{-1} K(X,X^*) \tag{21}$$

The prognostic framework is schematically depicted in Fig. 5. The model parameters $\theta = \{\sigma_f, \sigma_l, \sigma_n, c_1, c_0\}$ can be estimated by maximizing the marginal likelihood $logp(y|X,\theta) = -\frac{1}{2}y^T K_y^{-1} y - \frac{1}{2}\log|K_y| - \frac{n}{2}log2\pi$, where $K_y = K_f + \sigma_n^2 I$ is the covariance matrix of the noisy target y and K_f the covariance matrix of f. To maximize the marginal likelihood, we use the partial derivative with respect to parameters θ:

$$\underset{\theta}{argmax}\frac{\partial}{\partial\theta_j} logp(y|X,\theta) = \frac{1}{2}y^T K^{-1}\frac{\partial K}{\partial\theta_j}K^{-1}y - \frac{1}{2}tr(K^{-1}\frac{\partial K}{\partial\theta_j}) \tag{22}$$

After estimating the model parameters, the new data (HIs) are used as inputs to the trained GP model to predict the RUL.

4. Results and discussion

4.1. Genetic algorithm-based health indicator

The methodology described in Section 3.1 is used to create a hyper HI based on simpler HI inputs. The selected fusion equation that resulted after the optimization process; can be seen in eq. (23) and the fused HI from this point on will be noted as HI_{GA}.

$$HI_{GA} = vHI_1\left(HI_4 - \frac{vHI_2 + 0.5HI_3}{vHI_2}\right) + 1 \tag{23}$$

The monotonicity and prognosability of HI_{GA} for the training set are 0.89 and 0.95 respectively, both higher than those reported for the input HIs in Fig. 3. For the entire dataset (including the test data) the respective values are 0.84 and 0.91. HI_{GA} is presented in Fig. 6. HI_{GA} shows a highly monotonic and prognosable behavior not only for the training set (9 specimens) which was expected but also for the test set (5 specimens, dashed lines). As a result, the proposed GA fusion scheme can be characterized as successful. This is also evident from the improved fitness function values, where HI_{GA} has superior values compared to the previously developed HIs. Only vHI_1's fitness is comparable to HI_{GA}, and it rationalizes its participation in the fused HI of eq. (23). HI_{GA} is depicted in Fig. 6. The behaviors of the four HI inputs are presented in Figs. A1 and A2 of the Appendix.

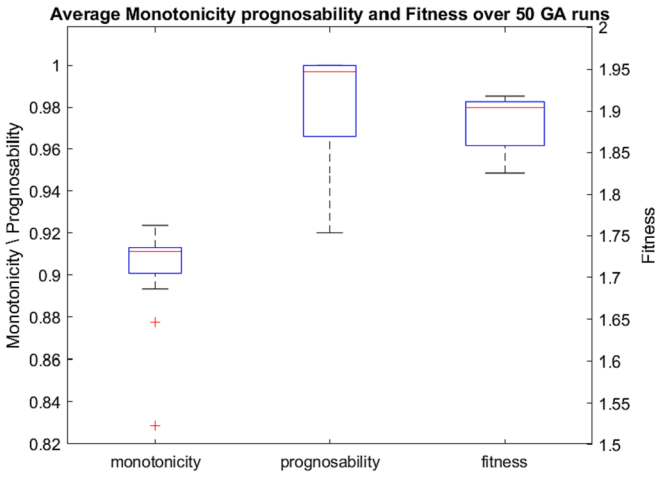

Fig. 7. Average monotonicity, prognosability and fitness with variance over 50 Genetic algorithm runs.

To evaluate the repeatability of the proposed methodology, the process was run multiple times with the exact same parameters. After 50 runs, some similar results were acquired, regarding inputs and fusion operators, yet the exact same function was not obtained. This result does not come as a surprise. Due to the nature of the optimization problem, there are multiple local optimums, which are achieved via different combination of the inputs. In Fig. 7 the average monotonicity, prognosability and overall fitness over the 50 runs is depicted. We can observe that the results show high values of monotonicity and prognosability with little scatter, hence the good feature level fusion can be replicated. This is also demonstrated by the low scatter of the overall fitness values.

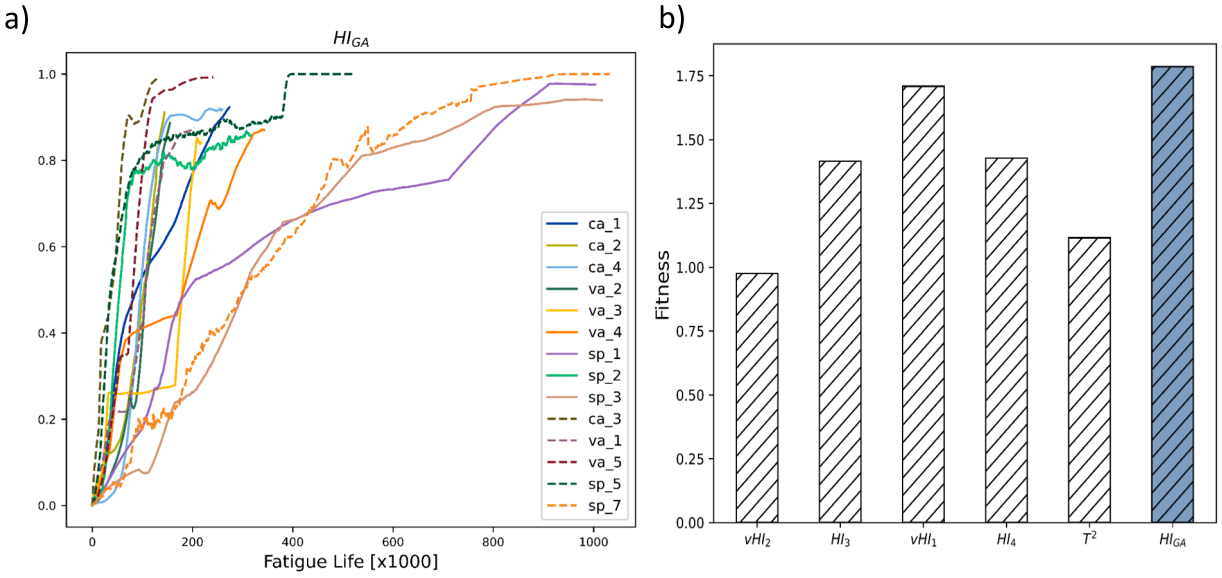

Fig. 6. a) HI_{GA} versus fatigue life. Panels used for training are depicted with solid lines, while those used for validation and testing are depicted with dashed lines. b) Fitness values of the various HIs including test set.

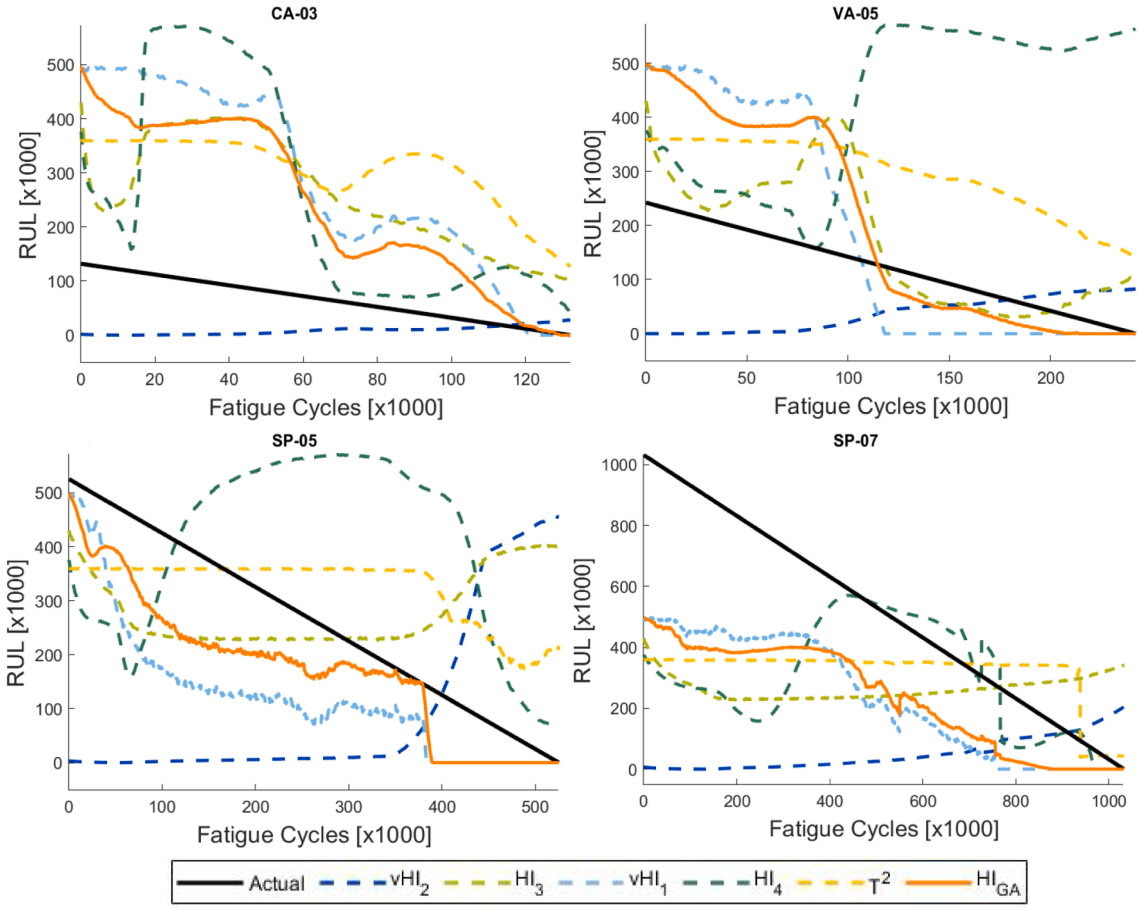

Fig. 8. RUL predictions for the test panels for the different HIs.

4.2. *Remaining useful life estimation*

To justify the necessity of the proposed fused HI_{GA} and demonstrate its superiority in predicting the RUL of the test panels, we utilize it for RUL prognostics using GP regression. RUL prognostics are also obtained with the HIs of eq. 4–8 for comparison purposes. Fig. 8 summarizes the results. Four out of five test panels are shown, omitting the specimen used for the GP parameter tuning. It is evident that HI_{GA} approximates the true RUL much more closely than the rest HIs. vHI_2 and T^2 predictions are not able to capture the true RUL. vHI_2 shows predictions close to zero from the beginning while the predicted RUL increases near EoL, which is attributed to the very poor prognosability of this particular HI, while the lack of monotonicity of T^2 (see Fig. A2) is also reflected in the poor RUL estimations. HI_3's performance is also not notable, since for CA-03 and VA-05 the RUL predictions are not converging to the true RUL, while for the two spectrum panels the estimations are extremely poor.

For the rest of the HIs, the RUL estimations are discussed more in depth. More specifically, for panels CA-03 and VA-05 HI_{GA} and vHI_1, display good RUL estimations, especially after 50 % of the lifetime, when they start to converge to the true RUL. Near the EoL both RUL estimations approach the actual RUL, with HI_{GA} showing slightly better estimations. While HI_4 shows relatively accurate RUL estimation for CA-03, for VA-05 the RUL shows an increasing trend, which is due to the sudden decrease in HI_4's values at that time for this specimen (see Fig. A1). HI_{GA} displays once again better RUL estimations converging to the true RUL close to the EoL, something that no other HI manages. For SP-05, HI_{GA} and vHI_1 show similar RUL estimations, both underestimating the true RUL, but HI_{GA} converges to the true RUL, before both HI_{GA} and vHI_1 suddenly drop to zero. For HI_3, the estimations display an increase near the EoL which is attributed to the drop in the HI's values. HI_4 even though at first has a shifting behavior between overestimating and underestimating the RUL near the EoL it manages to slightly converge to the true RUL. Finally, for panel SP-07 all HIs underestimate the RUL, and most of them manage to converge to the true RUL near the EoL, though HI_{GA} and vHI_1 show a more steady convergence.

It can be clearly seen that HI_{GA} is able to always converge to the true RUL near the EoL, unlike the rest of the HIs, demonstrating the effect of the high prognosability. The only other HI with similar prediction results is vHI_1, which is a core part of HI_{GA}, though HI_{GA} shows slightly better performance. Regarding the prognostic behavior of some HIs we note that GP is a regression algorithm which is mapping the HI value to a RUL value based on training data. Hence in cases like HI_4 for VA-05 where the HI values decrease, the regression model is mapping this decrease to a higher RUL.

Looking closely at Fig. 8, it is evident that HI_{GA} outperforms the rest of the HIs since it better follows the true RUL and particularly near the end-of-life. This by itself justifies the need for a methodology as the one discussed throughout the paper. To further assess the quality of the mean predictions and quantify the performance, several prognostic performance metrics, i.e. Mean Absolute Error (MAE), Mean Absolute Percentage Error (MAPE), Root Mean Square Error (RMSE), and Cumulative relative accuracy (CRA) (Eq. 24–27), are employed [57,58].

$$MAE = \frac{1}{N}\sum_{i=1}^{N}\left|RUL_i^* - RUL_i\right| \tag{24}$$

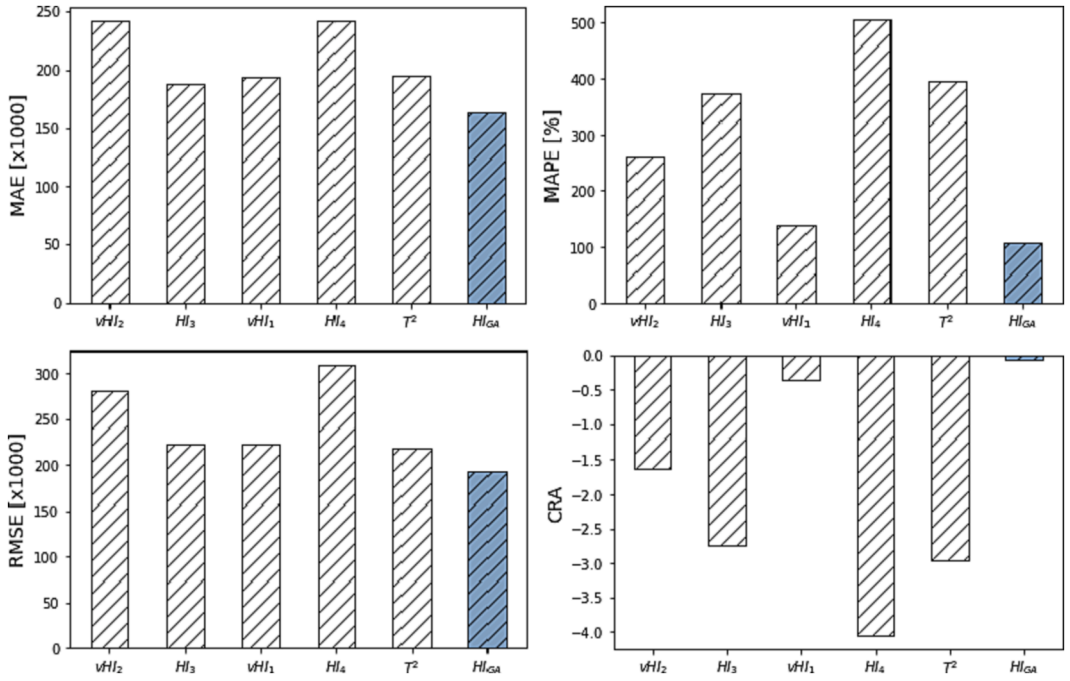

Fig. 9. Average prognostic performance metrics.

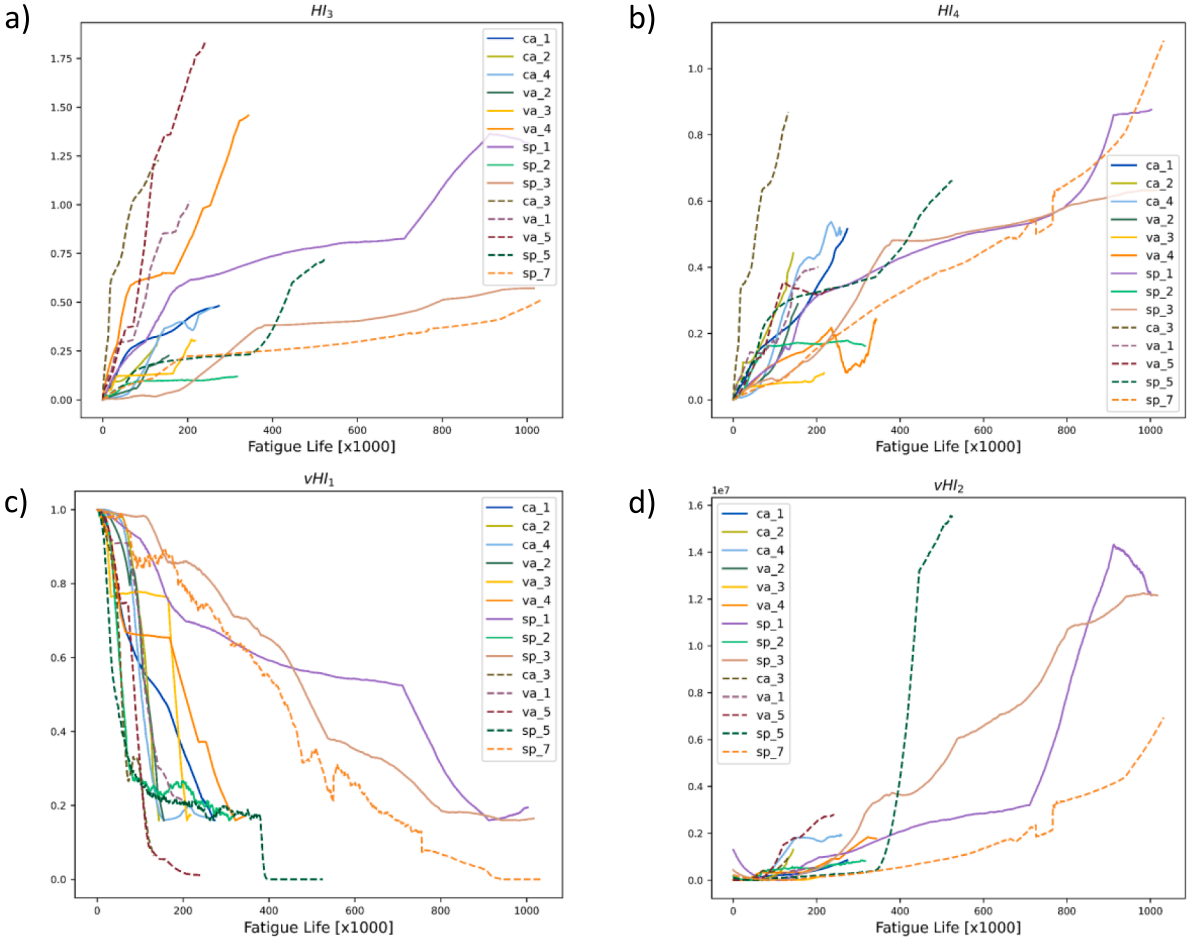

Fig. A1. HIs vs fatigue cycles for the different panels. Solid lines represent panels used for training, while dashed those used for testing. a) HI_3, b) HI_4, c) vHI_1, d) vHI_2.

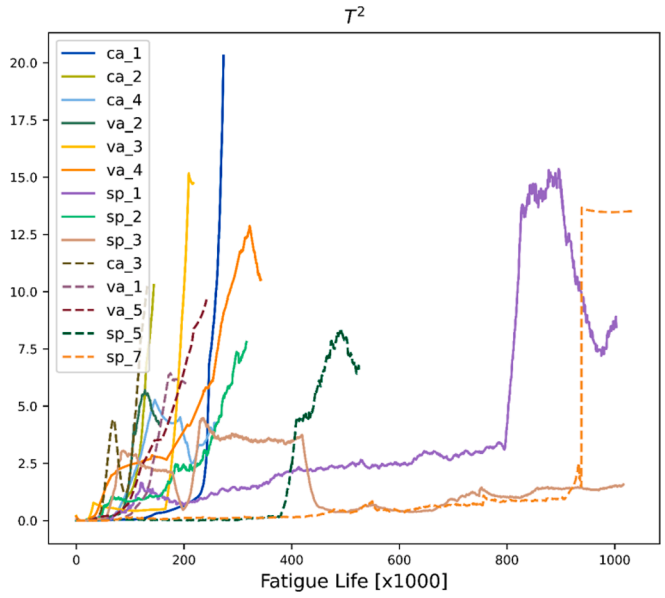

Fig. A2. T^2 vs fatigue cycles for the different panels. Solid lines represent panels used for the training process, while dashed those used for testing.

$$MAPE = \frac{1}{N}\sum_{i=1}^{N}\frac{|RUL_i^* - RUL_i|}{RUL_i} \times 100 \tag{25}$$

$$RMSE = \sqrt{\frac{1}{N}\sum_{i=1}^{N}\left(RUL_i^* - RUL_i\right)^2} \tag{26}$$

$$CRA = \frac{\sum_{i=1}^{N} RA_i}{N}, whereRA_i = 1 - |\frac{RUL_i^* - RUL_i}{RUL_i}| \tag{27}$$

where RUL_i *and* RUL_i^* are the true and predicted RUL at time *i*.

Fig. 9 summarizes the aforementioned metrics scores averaged across all the specimens of the test set. Evidently, HI_{GA} is outperforming the other HIs in all metrics. This result validates what was already visually observed in Fig. 8, verifying that HI_{GA} is an enhanced version of the previously proposed HIs and a more suitable HI for prognostic purposes.

5. Conclusions

In this paper, a novel strain-based Health Indicator is proposed for SHM data-driven RUL prognostics of composite structures. CFRP single-stiffened panels were subjected to a variety of compression-compression fatigue scenarios and FBG sensors were used to measure strain along the stiffeners' feet. Three different loading scenarios of increasing complexity were implemented, i.e., constant amplitude fatigue, variable amplitude fatigue, and random (spectrum) amplitude fatigue. A new health indicator is derived after a fusion of simpler HIs developed in previous work [33]. For the fusion procedure, genetic algorithms are employed in order to maximize the value of a fitness function comprising, with equal weight, of the average monotonicity and prognosability of the training dataset. Out of the 14 tested panels 9 were randomly chosen and were used to train the genetic algorithm and derive the fusion function while the rest were used to validate the result. The fused HI_{GA} displays superior monotonicity and prognosability compared to its constituent HIs.

All HIs are then utilized to estimate the RUL of the panels. Gaussian Process Regression is employed for the RUL prediction task. It is shown that the proposed HI_{GA} significantly outperforms its constituent HIs regarding RUL estimation and this is validated by employing some common prognostic performance metrics. The main advantage of the proposed methodology is that it is material agnostic and can thus be employed in any application where SHM data from a degrading structure are available.

Though the methodology has provided promising results in lab scale tests, its applicability in industrial environments still needs further consideration and validation. An industrial environment such as a real aircraft structure, is very challenging due to the complexity of loading and additional parameters such as environmental loads or unforeseen events (bird strikes). To deploy such methodologies in such environments we have to extend the methodology to take into account the effect of temperature/moisture fluctuations on the acquired strain data. Moreover, we have to convince the stakeholders (OEMs etc) that the sensing technologies are reliable and durable. The main drawback of this purely data-driven methodology is the dependence on the data quality. If the sensor readings are not representative of the degradation due to sensor failure or any other reason, then the proposed methodology might be prone to erroneous estimates, and this increases uncertainty, especially in real industrial situations.

Funding

The research work was supported by the Hellenic Foundation for Research and Innovation (H.F.R.I.) under the "First Call for H.F.R.I. Research Projects to support Faculty members and Researchers and the procurement of high-cost research equipment grant" (Project Number: 2573). A. Broer acknowledges funding from the European Union's Horizon 2020 research and innovation program (Grant No.769288, ReMAP project).

CRediT authorship contribution statement

Georgios Galanopoulos: Conceptualization, Methodology, Software, Formal analysis, Investigation, Data curation, Writing - original draft. **Nick Eleftheroglou:** Conceptualization, Software, Writing – review & editing. **Dimitrios Milanoski:** Conceptualization, Investigation. **Agnes Broer:** Investigation, Data curation. **Dimitrios Zarouchas:** Writing – review & editing. **Theodoros Loutas:** Conceptualization, Supervision, Writing – review & editing, Funding acquisition.

Declaration of Competing Interest

The authors declare that they have no known competing financial interests or personal relationships that could have appeared to influence the work reported in this paper.

Data availability

The data that has been used is confidential.

Acknowledgement

The authors would like to acknowledge the colleagues at Delft University of technology (Aerospace Structures and Materials Laboratory and Structural Integrity and Composites group) and University of Patras (Applied Mechanics Laboratory) for the technical support and the colleagues at Smartec SA for providing the optical fibers.

Appendix. Health indicators

In this appendix the HIs of eq. (4)-(7) that participate in HI_{GA} are presented (Fig. A1), since new panels have been added to the study. vHI_1 is presented after using the methodology described in section 3.1.

T^2 has not been discussed in [33] hence a brief overview is shown here. The procedure is similar to the one for calculating vHI_2.

- The mean and standard deviation of a set of Reference data $\mathbf{X_H}$ (initial values of each experiment) are used to scale the data $\mathbf{X}$
- Principal Component Analysis (PCA) model is created using $\mathbf{X_H}$, with $\mathbf{P}$ the eigenvalue vector used for the transformation $\boldsymbol{T_H = X_H P}$.
- The eigenvalues corresponding to 95 % explained variance ($\mathbf{P_r}$) are retained and used to transform the entire dataset $\mathbf{X}$ into $\boldsymbol{T = XP_R}$
- Then:

$$T^2 = \sum_{i=1}^{k} \frac{\tau_i^2}{\lambda_i} = \mathrm{T}\Lambda^{-1}\mathrm{T}^{\mathrm{T}}$$

T^2 is a measure of variability in the k first Principal Components. The behavior of T^2 can be seen in Fig. A2.

References

[1] Kassapoglou C. Design and analysis of composite structures: with applications to aerospace structures. John Wiley & Sons; 2013.
[2] Hey Leung MS, Corcoran J. A probabilistic method for structural integrity assurance based on damage detection structural health monitoring data. Struct Heal Monit 2022;21(4):1608–25.
[3] Sbarufatti C, Manes A, Giglio M. Application of sensor technologies for local and distributed structural health monitoring. Struct Control Heal Monit Jul. 2014;21 (7):1057–83. https://doi.org/10.1002/STC.1632.
[4] Marques R, Unel M, Yildiz M, Suleman A. Remaining useful life prediction of laminated composite materials using Thermoelastic Stress Analysis. Compos Struct 2019;210:381–90.
[5] Khodaei ZS, Aliabadi MH. A multi-level decision fusion strategy for condition based maintenance of composite structures. Mater. 2016, Vol. 9, Page 790, vol. 9, no. 9, p. 790, Sep. 2016, doi: 10.3390/MA9090790.
[6] Lima RAA, Perrone R, Carboni M, Bernasconi A. Experimental analysis of mode I crack propagation in adhesively bonded joints by optical backscatter reflectometry and comparison with digital image correlation. Theor Appl Fract Mech 2021;116: 103117. https://doi.org/10.1016/j.tafmec.2021.103117.
[7] Loutas T, Eleftheroglou N, Zarouchas D. A data-driven probabilistic framework towards the in-situ prognostics of fatigue life of composites based on acoustic emission data. Compos Struct 2017;161:522–9. https://doi.org/10.1016/j.compstruct.2016.10.109.
[8] Eleftheroglou N, Zarouchas DS, Loutas TH, Alderliesten RC, Benedictus R. Online remaining fatigue life prognosis for composite materials based on strain data and stochastic modeling. Key Eng Mater 2016;713:34–7.
[9] Saxena A, Goebel K, Larrosa CC, Janapati V, Roy S, Chang F-K. Accelerated aging experiments for prognostics of damage growth in composite materials. National aeronautics and space administration moffett field ca ames research …, 2011.
[10] Ling Y, Mahadevan S. Integration of structural health monitoring and fatigue damage prognosis. Mech Syst Signal Process 2012;28:89–104.
[11] Sikorska JZ, Hodkiewicz M, Ma L. Prognostic modelling options for remaining useful life estimation by industry. Mech Syst Signal Process 2011;25(5):1803–36. https://doi.org/10.1016/j.ymssp.2010.11.018.
[12] Lei Y, Li N, Guo L, Li N, Yan T, Lin J. Machinery health prognostics: A systematic review from data acquisition to RUL prediction. Mech Syst Signal Process 2018; 104:799–834.
[13] Philippidis TP, Vassilopoulos AP. Fatigue strength prediction under multiaxial stress. J Compos Mater 1999;33(17):1578–99.
[14] Wu F, Yao W. A fatigue damage model of composite materials. Int J Fatigue 2010; 32(1):134–8.
[15] Chiachıo J, Chiachıo M, Saxena A, Rus G, Goebel K. An energy-based prognostics framework to predict fatigue damage evolution in composites. In: Proceedings of the annual conference of the prognostics and health management society, 2013, vol. 1, pp. 363–371.
[16] Chiachío M, Chiachío J, Rus G, Beck JL. Predicting fatigue damage in composites: A Bayesian framework. Struct Saf 2014;51:57–68. https://doi.org/10.1016/j.strusafe.2014.06.002.
[17] Peng T, Liu Y, Saxena A, Goebel K. In-situ fatigue life prognosis for composite laminates based on stiffness degradation. Compos Struct 2015;132:155–65. https://doi.org/10.1016/j.compstruct.2015.05.006.
[18] Colombo L, Oboe D, Sbarufatti C, Cadini F, Russo S, Giglio M. Shape sensing and damage identification with iFEM on a composite structure subjected to impact damage and non-trivial boundary conditions. Mech Syst Signal Process 2021;148: 107163.
[19] Eleftheroglou N, Zarouchas D, Loutas T, Alderliesten R, Benedictus R. Structural health monitoring data fusion for in-situ life prognosis of composite structures. Reliab Eng Syst Saf 2018;178:40–54. https://doi.org/10.1016/j.ress.2018.04.031.
[20] Liu Y, Mohanty S, Chattopadhyay A. A Gaussian process based prognostics framework for composite structures. In: Modeling, signal processing, and control for smart structures 2009, 2009, vol. 7286, p. 72860J.
[21] Liu Y, Mohanty S, Chattopadhyay A. Condition based structural health monitoring and prognosis of composite structures under uniaxial and biaxial loading. J Nondestruct Eval 2010;29(3):181–8. https://doi.org/10.1007/s10921-010-0076-2.
[22] Loutas T, Eleftheroglou N, Georgoulas G, Loukopoulos P, Mba D, Bennett I. Valve failure prognostics in reciprocating compressors utilizing temperature measurements, PCA-based data fusion, and probabilistic algorithms. IEEE Trans Ind Electron 2019;67(6):5022–9.
[23] Baraldi P, Bonfanti G, Zio E. Differential evolution-based multi-objective optimization for the definition of a health indicator for fault diagnostics and prognostics. Mech Syst Signal Process 2018;102:382–400.
[24] Medjaher K, Zerhouni N, Baklouti J. Data-driven prognostics based on health indicator construction: Application to PRONOSTIA's data. European Control Conference (ECC) 2013;2013:1451–6.
[25] Hu C, Youn BD, Wang P, Taek Yoon J. Ensemble of data-driven prognostic algorithms for robust prediction of remaining useful life. Reliab Eng Syst Saf Jul. 2012;103:120–35. https://doi.org/10.1016/j.ress.2012.03.008.
[26] Wen P, Zhao S, Chen S, Li Y. A generalized remaining useful life prediction method for complex systems based on composite health indicator. Reliab Eng Syst Saf 2021;205:107241.
[27] Duong B, Khan S, Shon D, Im K, Park J, Lim D-S, et al. A reliable health indicator for fault prognosis of bearings. Sensors (Switzerland) Nov. 2018;18(11):3740.
[28] Lei Y, Li N, Lin J. A new method based on stochastic process models for machine remaining useful life prediction. IEEE Trans Instrum Meas 2016;65(12):2671–84.
[29] Milanoski DP, Loutas TH. Strain-based health indicators for the structural health monitoring of stiffened composite panels. J Intell Mater Syst Struct Feb. 2021;32 (3):255–66. https://doi.org/10.1177/1045389X20924822.
[30] Milanoski D, Galanopoulos G, Broer A, Zarouchas D, Loutas T. A strain-based health indicator for the SHM of skin-to-stringer disbond growth of composite stiffened panels in fatigue. In: European Workshop on Structural Health Monitoring, 2020, pp. 626–635.
[31] Loukopoulos P, Zolkiewski G, Bennett I, Sampath S, Pilidis P, Duan F, et al. Reciprocating compressor prognostics of an instantaneous failure mode utilising temperature only measurements. Appl Acoust 2019;147:77–86.
[32] Shahid N, Ghosh A. TrajecNets: online failure evolution analysis in 2D space. United Technol. Res. Center, Penrose Wharf, Penrose Bus. Center, Cork, Irel., 2019.
[33] Galanopoulos G, Milanoski D, Broer A, Zarouchas D, Loutas T. Health monitoring of aerospace structures utilizing novel health indicators extracted from complex strain and acoustic emission data. Sensors 2021;21(17):5701.
[34] Yang F, Habibullah MS, Zhang T, Xu Z, Lim P, Nadarajan S. Health index-based prognostics for remaining useful life predictions in electrical machines. IEEE Trans Ind Electron 2016;63(4):pp. https://doi.org/10.1109/TIE.2016.2515054.
[35] Song C, Liu K, Zhang X. Integration of data-level fusion model and kernel methods for degradation modeling and prognostic analysis. IEEE Trans Reliab Jun. 2018;67 (2):640–50. https://doi.org/10.1109/TR.2017.2715180.
[36] Liu D, Zhou J, Liao H, Peng Y, Peng X. A health indicator extraction and optimization framework for lithium-ion battery degradation modeling and prognostics. IEEE Trans Syst Man Cybern Syst 2015;5(6):915–28. https://doi.org/10.1109/TSMC.2015.2389757.
[37] Chen Z, Xia T, Zhou D, Pan E. A health index construction framework for prognostics based on feature fusion and constrained optimization. IEEE Trans Instrum Meas 2021;70:3523315. https://doi.org/10.1109/TIM.2021.3104414.
[38] Azevedo D, Cardoso A, Ribeiro B. Estimation of health indicators using advanced analytics for prediction of aircraft systems remaining useful lifetime. PHM Soc. Eur. Conf., vol. 5, no. 1, pp. 10–10, Jul. 2020, doi: 10.36001/PHME.2020.V5I1.1226.
[39] Nguyen KTP, Medjaher K. An automated health indicator construction methodology for prognostics based on multi-criteria optimization. ISA Trans Jul. 2021;113:81–96. https://doi.org/10.1016/j.isatra.2020.03.017.
[40] Milanoski D, Galanopoulos G, Zarouchas D, Loutas T. Multi-level damage diagnosis on stiffened composite panels based on a damage-uninformative digital twin. Struct Heal Monit Jul. 2022:1–23. https://doi.org/10.1177/14759217221108676/ASSET/IMAGES/LARGE/10.1177_14759217221108676-FIG18.JPEG.
[41] Glisic B, Inaudi D. Development of method for in-service crack detection based on distributed fiber optic sensors. Struct Heal Monit An Int J 2011;11(2):161–71. https://doi.org/10.1177/1475921711414233.

[42] Milanoski DP, Galanopoulos GK, Loutas TH. Digital-twins of composite aerostructures towards structural health monitoring. 2021 IEEE Int. Work. Metrol. AeroSpace, Metroaerosp. 2021 - Proc., pp. 613–618, Jun. 2021, doi: 10.1109/METROAEROSPACE51421.2021.9511653.
[43] Broer A, Galanopoulos G, Benedictus R, Loutas T, Zarouchas D. Fusion-based damage diagnostics for stiffened composite panels. Struct. Heal. Monit., p. 14759217211007128, 2021.
[44] Yue N, Broer A, Briand W, Rébillat M, Loutas T, Zarouchas D. Assessing stiffness degradation of stiffened composite panels in post-buckling compression-compression fatigue using guided waves. Compos Struct 2022;293:115751.
[45] Milanoski D, Galanopoulos G, Zarouchas D, Loutas T. Damage diagnostics on post-buckled stiffened panels utilizing the digital-twin concept. Lect Notes Civ Eng 2023;vol. 253 LNCE:213–22. https://doi.org/10.1007/978-3-031-07254-3_21/FIGURES/6.
[46] Zarouchas D, Broer A, Galanopoulos G, Briand W, Benedictus R, Loutas T. Compression Compression fatigue tests on single stiffener aerospace structures. DataverseNL, doi: doi:10.34894/QNURER.
[47] De Jong JB, Schütz D, Lowak H, Schijve J. A standardized load sequence for flight simulation tests on transport aircraft wing structures. NLR-TR 73029 U, LBF Bericht FB-106, 1973.
[48] Coble J, Hines JW. Identifying optimal prognostic parameters from data: a genetic algorithms approach. In: Annual Conference of the PHM Society, 2009, vol. 1, no. 1.
[49] Firpi H, Vachtsevanos G. Genetically programmed-based artificial features extraction applied to fault detection. Eng Appl Artif Intell Jun. 2008;21(4):558–68. https://doi.org/10.1016/j.engappai.2007.06.004.
[50] Liao L. Discovering prognostic features using genetic programming in remaining useful life prediction. IEEE Trans Ind Electron 2014;61(5):2464–72. https://doi.org/10.1109/TIE.2013.2270212.
[51] Galanopoulos G, Eleftheroglou N, Milanoski, Broer A, Zarouchas D, Loutas T. An SHM data-driven methodology for the remaining useful life prognosis of aeronautical subcomponents, pp. 244–253, 2023, doi: 10.1007/978-3-031-07254-3_24.
[52] Silva S, Almeida J. GPLAB-a genetic programming toolbox for MATLAB. In: Proceedings of the Nordic MATLAB conference, 2003, pp. 273–278.
[53] Liu D, Pang J, Zhou J, Peng Y, Pecht M. Prognostics for state of health estimation of lithium-ion batteries based on combination Gaussian process functional regression. Microelectron Reliab Jun. 2013;53(6):832–9. https://doi.org/10.1016/J.MICROREL.2013.03.010.
[54] Li M, Sadoughi M, Shen S, Hu C. Remaining useful life prediction of lithium-ion batteries using multi-model Gaussian process. 2019 IEEE Int Conf Progn Heal Manag ICPHM Jun. 2019;2019. https://doi.org/10.1109/ICPHM.2019.8819384.
[55] Benker M, Bliznyuk A, Zaeh MF. A Gaussian process based method for data-efficient remaining useful life estimation. IEEE Access 2021;9:137470–82. https://doi.org/10.1109/ACCESS.2021.3116813.
[56] Williams CK, Rasmussen CE. Gaussian processes for machine learning, vol. 2, no. 3. Cambridge, MA: MIT press; 2006.
[57] Saxena A, et al. Metrics for evaluating performance of prognostic techniques. In: 2008 international conference on prognostics and health management, 2008, pp. 1–17.
[58] Saxena A, Celaya J, Saha B, Saha S, Goebel K. Metrics for offline evaluation of prognostic performance. Int J Progn Heal Manag 2010;1(1):4–23.